Current Marching Technique for Electromagnetic Scattering Computations

Andrew A. Zaporozhets and Mireille F. Levy, *Member, IEEE*

***Abstract*— An iterative solver is used to compute the electromagnetic field scattered by perfectly conducting three-dimensional (3-D) objects of arbitrary shape. The unique solution of the dual-surface integral equation is approached by successive forward/backward calculations of the current. Convergence is very fast, giving accurate results in about a dozen iterations for convex objects. The method handles successfully single and multiple objects, convex objects, and cavities. Calculations can be carried out on a desktop computer for relatively large objects, with dimensions of ten wavelengths and more.**

***Index Terms*— Electromagnetic scattering, integral equation method, radar cross section.**

I. Introduction

In this paper, we are concerned with electromagnetic scattering by perfectly conducting objects. A number of integral equation methods for solving scattering problems in the frequency domain have been described in the literature [1].

Iterative methods with extremely fast convergence (in just a few iterations) have recently been applied to scattering by open rough surfaces [2]–[4] and to acoustic scattering [5]. The methods in [2]–[4] are based on the forward/backward updating procedure for the surface electric current. In [2], this technique was called the method of ordered multiple interactions (MOMI). We discovered this idea independently, stimulated by our work on parabolic equation methods [6], [7] and applied it to scattering by closed bodies in three dimensions. We use the phrase current marching technique (CMT) to describe the method. Forward current marching is very similar to the forward marching of the field in parabolic equation techniques. The parabolic approximation splits the vector wave equation into two terms corresponding to forward and backward propagation, respectively, and these can be solved by marching methods. However, current marching does not have the paraxial limitations of the parabolic equation method and also has the great advantage that iteration automatically deals with the coupling between backward and forward generated currents.

The main difficulty was that the method in its original (similar to [2]–[4]) formulation did not converge for a closed surface. The solution is to use the dual-surface magnetic field equation [8], [9], which is not plagued by the internal resonance problems (for some references on the internal resonance problem see [10]). The second internal surface acts as an absorber for the field inside the object.

Manuscript received March 11, 1998; revised March 12, 1999.

The authors are with the Radio Communications Research Unit, Rutherford Appleton Laboratory, Chilton, Didcot, OX11 0QX U.K.

Publisher Item Identifier S 0018-926X(99)05810-X.

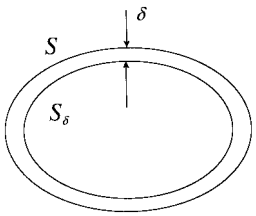

Fig. 1. Geometry for dual-surface integral equation.

The method converges very fast, in about a dozen iterations for convex objects. By using conditioning techniques, convergence of the CMT algorithm is obtained for nonconvex bodies.

The dual-surface integral equations are given in Section II. Section III describes the CMT iterative solver and Section IV discusses a number of examples, including spheres, double spheres, cubes, and a semi-open cavity.

II. Dual-Surface Integral Equations

We work with the dual-surface integral equation for the magnetic field [8], [9]. For a perfect conductor with smooth surface S, we define the surface S_δ as in Fig. 1. For small enough δ, this surface is inside S. We define a natural correspondence between points on S and points on S_δ by associating point $\mathbf{r}$ on S with point $\mathbf{r}-\delta\mathbf{n}$ on S_δ, where $\mathbf{n}$ is the outer normal to the surface S at point $\mathbf{r}$.

We assume harmonic dependence of the fields on time. Let $\mathbf{H}_i$ be the incident magnetic field and let α be a real number. We define the following hybrid field, which is a combination of the magnetic fields on S and S_δ

$$\mathbf{H}_0(\mathbf{r}) = \mathbf{H}_i(\mathbf{r}) - i\alpha\mathbf{H}_i(\mathbf{r}-\delta\mathbf{n}). \tag{1}$$

We also define the hybrid Green's function

$$G_0(\mathbf{r},\mathbf{r}') = G(\mathbf{r},\mathbf{r}') - i\alpha G(\mathbf{r}-\delta\mathbf{n},\mathbf{r}') \tag{2}$$

where G is the three-dimensional (3-D) Green's function for the Helmholtz equation in vacuum

$$G(\mathbf{r},\mathbf{r}') = \frac{e^{ik|\mathbf{r}-\mathbf{r}'|}}{4\pi|\mathbf{r}-\mathbf{r}'|}. \tag{3}$$

Here, $|\mathbf{r}|$ stands for the magnitude or 3-D Euclidian norm of the vector $\mathbf{r}$ and k is the vacuum wave number. We now look

at the dual-surface magnetic field integral equation for the current density $\mathbf{K}$

$$\mathbf{n}\times\mathbf{H}_0(\mathbf{r})=\frac{1}{2}\mathbf{K}(\mathbf{r})-\mathbf{n}\times\int_S\mathbf{K}(\mathbf{r}')\times\operatorname{grad}_{\mathbf{r}'}(G_0(\mathbf{r},\mathbf{r}'))\,dS(\mathbf{r}'). \quad (4)$$

The integral is an improper integral, taken in the sense of Cauchy principal value. For real α and small enough δ, (4) has a unique solution [8], regardless of whether k corresponds to a resonant frequency of the interior problem for S. Since the current corresponding to the unique solution to Maxwell's equations for incident fields $\mathbf{E}_i,\mathbf{H}_i$ automatically satisfies (4), the unique solution of (4) is the desired current. Choices of α between 0.5 and 1, and δ close to $\lambda/4$, where λ is the wavelength of the incident field, give good results. In what follows, we use $\alpha=0.5$ and $\delta=\lambda/4$.

We briefly recall the reasons why the dual-surface integral equation is well behaved. A detailed proof is given in [8]. The uniqueness property is based on the fact that boundary conditions are effectively enforced on both surfaces. By linearity, if two currents $\mathbf{K}_1$ and $\mathbf{K}_2$ are solutions of (4) then the magnetic field $\mathbf{H}$ radiated by the difference current $\mathbf{K}=\mathbf{K}_2-\mathbf{K}_1$ satisfies the vector wave equation and for any $\mathbf{r}$ on S we have

$$\mathbf{H}(\mathbf{r})-i\alpha\mathbf{H}(\mathbf{r}-\delta\mathbf{n})=0. \quad (5)$$

If δ is small enough, the phase of $\mathbf{H}$ will not vary much between the two surfaces. For real α this implies that $\mathbf{H}$ is zero on both surfaces. If δ is less than $\lambda/2$, one can then use waveguide arguments to conclude that $\mathbf{H}$ is zero everywhere because the cavity formed by S and S_δ cannot support any resonant modes. Hence, $\mathbf{K}$ is zero, too, and unicity is proved.

III. Iterative Current Marching

We denote by T the operator

$$T\mathbf{F}(\mathbf{r})=2\mathbf{n}\times\int_S\mathbf{F}(\mathbf{r}')\times\operatorname{grad}_{\mathbf{r}'}(G_0(\mathbf{r},\mathbf{r}'))\,dS(\mathbf{r}'). \quad (6)$$

The operator T is defined on suitably smooth vector functions $\mathbf{F}$ on the surface S. It is clear that the current density we seek is the unique solution to

$$\{(I-T)\mathbf{F}\}(\mathbf{r})=2\mathbf{n}\times\mathbf{H}_0(\mathbf{r}). \quad (7)$$

In other words, we need to invert the operator $I-T$. We now define a discretized version of T as follows: first discretize the surface S into patches S_j with centers $(\mathbf{r}_1,\mathbf{r}_2,\cdots,\mathbf{r}_N)$. We put

$$\mathbf{C}_{ij}=\int_{S_j}\operatorname{grad}_{\mathbf{r}'}(G_0(\mathbf{r}_i,\mathbf{r}'))\,dS(\mathbf{r}'). \quad (8)$$

The discretized version U of T is obtained by assuming that the current is constant on each patch. It is defined on discrete functions $\tilde{\mathbf{F}}=(\mathbf{F}_1,\mathbf{F}_2,\cdots,\mathbf{F}_N)$ representing the current at points $(\mathbf{r}_1,\mathbf{r}_2,\cdots,\mathbf{r}_N)$ by putting

$$(U\tilde{\mathbf{F}})_i=2\sum_{j=1}^{N}\mathbf{n}_i\times(\mathbf{F}_j\times\mathbf{C}_{i,j}). \quad (9)$$

In the method of moment terminology, this corresponds to pulse basis functions, using delta functions as testing functions. If the size of the patches is small enough, U is a good approximation of T and the linear system

$$\{(I-U)\tilde{\mathbf{F}}\}_i=2\mathbf{n}_i\times\mathbf{H}_0(\mathbf{r}_i),\quad i=1,\cdots,N \quad (10)$$

has a unique solution which is close to the desired solution $\mathbf{K}$ of the continuous integral equation.

Current marching technique solves the system of linear equations (10) by an iteration process that computes successive induced currents. These are marched forward and backward relative to the direction of the incident wave until convergence is obtained.

Working with Cartesian coordinates (x,y,z), we assume that the incident field propagates along the positive x direction. We now use this direction as our splitting direction for the forward/backward iteration. From now on, we assume our grid points $(\mathbf{r}_1,\mathbf{r}_2,\cdots,\mathbf{r}_N)$ are ordered in increasing ranges x.

We define the local updating operator V_i at point $\mathbf{r}_i$ by

$$\begin{aligned}(V_i\tilde{\mathbf{F}})_i&=2\mathbf{n}_i\times\mathbf{H}_0(\mathbf{r}_i)+2\sum_{j=1}^{N}\mathbf{n}_i\times(\mathbf{F}_j\times\mathbf{C}_{i,j})\\(V_i\tilde{\mathbf{F}})_j&=\mathbf{F}_j,\quad j\neq i.\end{aligned} \quad (11)$$

Hence, V_i replaces the current at point $\mathbf{r}_i$ by the current induced by the magnetic field radiated by the old current without modifying the current at other points. This corresponds to Gauss–Seidel iteration of the process, updating one point at a time [11]. We are now going to define forward and backward operators A and B by applying these local operators repeatedly to points with increasing and decreasing ranges, respectively. We define $A\tilde{\mathbf{F}}=\tilde{\mathbf{G}}$ inductively by

$$\begin{aligned}\mathbf{G}_1&=2\mathbf{n}_1\times\mathbf{H}_0(\mathbf{r}_1)+2\sum_{j=1}^{N}\mathbf{n}_1\times(\mathbf{F}_j\times\mathbf{C}_{1,j})\\\mathbf{G}_2&=2\mathbf{n}_2\times\mathbf{H}_0(\mathbf{r}_2)+2\mathbf{n}_2\times(\mathbf{G}_1\times\mathbf{C}_{2,1})\\&\quad+2\sum_{j=2}^{N}\mathbf{n}_2\times(\mathbf{F}_j\times\mathbf{C}_{2,j})\\&\vdots\\\mathbf{G}_i&=2\mathbf{n}_i\times\mathbf{H}_0(\mathbf{r}_i)+2\sum_{j=1}^{i-1}\mathbf{n}_i\times(\mathbf{G}_j\times\mathbf{C}_{i,j})\\&\quad+2\sum_{j=i}^{N}\mathbf{n}_i\times(\mathbf{F}_j\times\mathbf{C}_{i,j})\\&\vdots\\\mathbf{G}_N&=2\mathbf{n}_N\times\mathbf{H}_0(\mathbf{r}_N)+2\sum_{j=1}^{N-1}\mathbf{n}_N\times(\mathbf{G}_j\times\mathbf{C}_{N,j})\\&\quad+2\mathbf{n}_N\times(\mathbf{F}_N\times\mathbf{C}_{N,1}).\end{aligned} \quad (12)$$

In other words, we have applied the local updating operators successively to all points in increasing range order

$$\tilde{\mathbf{G}}=V_NV_{N-1}\cdots V_1\tilde{\mathbf{F}}. \quad (13)$$

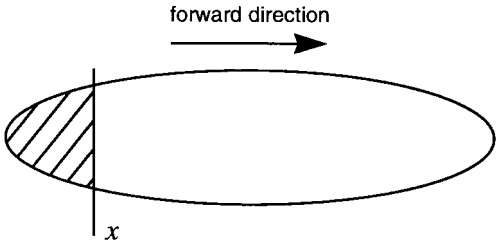

Fig. 2. Schematic representation of current marching technique. In the white area, the current has not yet been updated. In the striped area before range x, the current has already been marched forward.

Physically, this corresponds to marching the $\mathbf{F}$ current forward in range, as illustrated in Fig. 2. We start off with $\mathbf{F}$. We update the magnetic field and the current at successive ranges, replacing the current a given range by that induced by the new magnetic field values before that range and the old field values after that range. Similarly, we can define $B\tilde{\mathbf{F}} = \tilde{\mathbf{G}}$ by

$$\begin{aligned}
\mathbf{G}_N &= 2\mathbf{n}_N \times \mathbf{H}_0(\mathbf{r}_N) + 2\sum_{j=1}^{N} \mathbf{n}_N \times (\mathbf{F}_j \times \mathbf{C}_{N,j}) \\
\mathbf{G}_{N-1} &= 2\mathbf{n}_{N-1} \times \mathbf{H}_0(\mathbf{r}_{N-1}) \\
&\quad + 2\mathbf{n}_{N-1} \times (\mathbf{G}_N \times \mathbf{C}_{N-1,N}) \\
&\quad + 2\sum_{j=i}^{N-1} \mathbf{n}_{N-1} \times (\mathbf{F}_j \times \mathbf{C}_{N-1,j}) \\
&\vdots \\
\mathbf{G}_i &= 2\mathbf{n}_i \times \mathbf{H}_0(\mathbf{r}_i) + 2\sum_{j=i+1}^{N} \mathbf{n}_i \times (\mathbf{G}_j \times \mathbf{C}_{i,j}) \\
&\quad + 2\sum_{j=1}^{i} \mathbf{n}_i \times (\mathbf{F}_j \times \mathbf{C}_{i,j}) \\
&\vdots \\
\mathbf{G}_1 &= 2\mathbf{n}_1 \times \mathbf{H}_0(\mathbf{r}_1) + 2\sum_{j=1}^{N-1} \mathbf{n}_1 \times (\mathbf{G}_j \times \mathbf{C}_{1,j}).
\end{aligned} \tag{14}$$

So we have again applied the local updating operators repeatedly, this time marching back

$$\tilde{\mathbf{G}} = V_1 V_2 \cdots V_N \tilde{\mathbf{F}}. \tag{15}$$

We now define a sequence of functions as follows. We start with $\tilde{\mathbf{F}}^0 = 0$ and for nonnegative n, we put

$$\begin{aligned}
\tilde{\mathbf{F}}^{2n+1} &= A\tilde{\mathbf{F}}^{2n} \\
\tilde{\mathbf{F}}^{2n+2} &= B\tilde{\mathbf{F}}^{2n+1}.
\end{aligned} \tag{16}$$

In other words, $\tilde{\mathbf{F}}^1$ is the marched forward current induced by the hybrid incident field $\tilde{\mathbf{F}}^2$, the current marched back from $\tilde{\mathbf{F}}^1$, and so on. It is easy to see that if the sequence $(\tilde{\mathbf{F}}^n)$ converges, the limit will be the desired inverse of the operator $I - U$.

It turns out that for convex objects, the sequence does converge and that convergence is very rapid. Excellent accuracy is attained with a very small number of iterations regardless of object size or shape, as we shall see in the examples below. However, the sequence does not converge in general for nonconvex objects and we must seek a modified version of the algorithm.

We notice that for any fixed number t we can replace the operators A and B by A_t and B_t defined by

$$\begin{aligned}
A_t\tilde{\mathbf{F}} &= t\tilde{\mathbf{F}} + (1-t)A\tilde{\mathbf{F}} \\
B_t\tilde{\mathbf{F}} &= t\tilde{\mathbf{F}} + (1-t)B\tilde{\mathbf{F}}.
\end{aligned} \tag{17}$$

If the corresponding sequence converges, it will also be to the desired value. For both convex and nonconvex objects, values of t strictly between zero and one produce a converging sequence. This behavior would be readily explained if the spectral radius of the linear operator T was, at most, one [12]: since one is not an eigenvalue of T, the operator T_t would then have spectral radius strictly less than one and $I - T_t$ could be inverted by an iterative procedure, writing formally the Neumann series

$$(I - T_t)^{-1}\tilde{\mathbf{F}} = \sum_{n=0}^{\infty} T_t^n \tilde{\mathbf{F}}. \tag{18}$$

The forward/backward marching procedure is equivalent to computing this series. If the first guess $T\tilde{\mathbf{F}}$ does not have any components corresponding to spectral values of modulus one, as is probably the case for convex objects, the series will converge for $t = 0$. However, in general convergence is not guaranteed for $t = 0$ and we have to use a positive value of t. We found that in general, the best results are obtained for $t = 1/3$, which would be expected if the eigenvalues of T were all real and located between -1 and 0.

Since the required number of iterations does not depend on object size, execution times are of the order of N^2, which means that relatively large objects are still tractable on a desktop computer. We would like to point out that the marching nature of the method is essential for fast convergence: with Jacobi iteration where all the points are updated at once [11], the method fails. It is also worth pointing out that the forward/backward sequence fails to converge when the dual-surface quantities $G_0, \mathbf{H}_0$ are replaced with the single surface G and $\mathbf{H}_i$: the reason for this is that because of discretization, parasitic resonance always interferes with the results, producing an internal field which blows up instead of decaying to zero. We believe that the second surface acts like an absorbing layer which damps the internal field in the manner of the Bérenger perfectly matched layer [13].

Even though the single-surface iteration fails to converge, interesting results are obtained with a single forward iteration. For convex objects, this single-surface forward CMT (or SCMT) provides quite a good approximation to the forward scattered field. This is similar to the forward marching parabolic equation solution [6], [7].

IV. Examples

In all that follows, the incident field is a plane wave of amplitude one, vertically polarized. We use rectangular patches with maximum dimensions $\lambda/10$ to mesh the surfaces. Due to

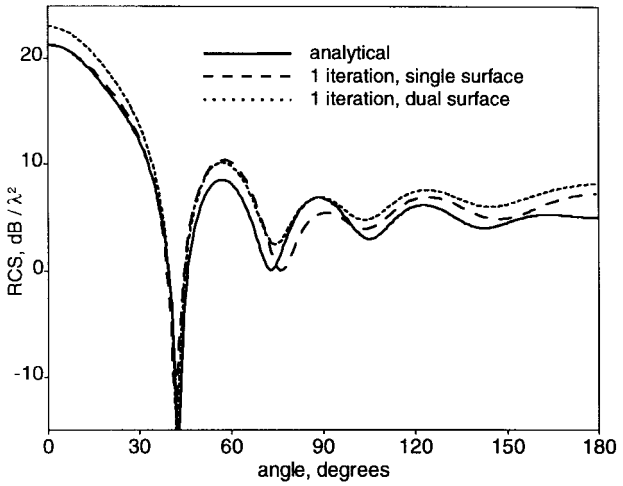

(a)

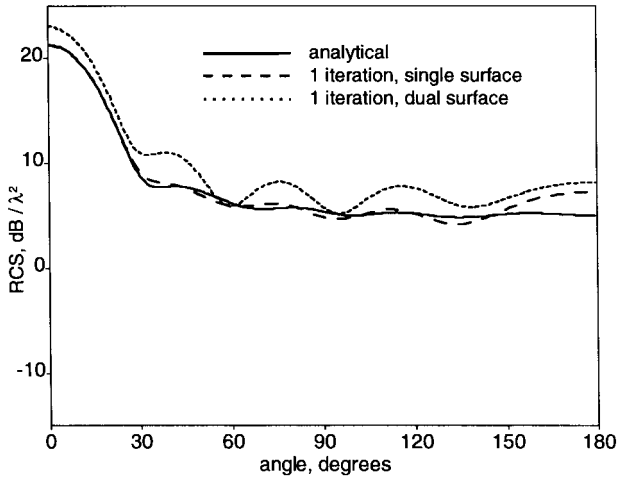

(b)

Fig. 3. Single iteration of CMT for sphere of radius λ. (a) Vertical plane pattern. (b) Horizontal plane pattern.

PC memory limitations (a Pentium 200 MHz PC with 64 Mb memory was used) we did not store the linear system matrix [see (10)] but recomputed it at each iteration. Because of the small number of iterations required, the penalty on integration time is acceptable.

We first look at convex bodies for which the standard CMT algorithm is convergent. Perfectly conducting spheres provide a good test of the method since theoretical solutions in the form of Mie expansions [14] are available for comparison. We start with a sphere of radius λ. Fig. 3 shows the RCS results obtained with the forward SCMT and also with a single forward iteration of the dual-surface CMT. For comparison, the theoretical solution is also shown. Fig. 3(a) and (b) shows results for the horizontal and vertical polarization planes, respectively. The first CMT iteration does not give as good an approximation as SCMT, which is understandable since it corresponds to the current induced by the dual-surface magnetic field and Green's function, rather than the more physical single-surface quantities. SCMT provides quite a good approximation for forward scatter for scattering angles up to 120° or so.

TABLE I
BEHAVIOR OF CMT SOLUTION FOR SPHERE OF RADIUS λ

Iter	Max current difference	Max internal magnetic field	Max error in radiation pattern for vertical plane (dB)	Max error in radiation pattern for horizontal plane (dB)
1	2.996	0.999	3.13	3.29
2	2.867	0.278	1.03	2.23
3	0.256	0.101	0.71	0.68
4	0.093	0.048	0.31	0.40
5	0.038	0.037	0.18	0.25
6	0.015	0.033	0.18	0.20
7	0.008	0.033	0.16	0.17
8	0.002	0.033	0.16	0.17
9	0.001	0.033	0.16	0.16
10	0.000	0.033	0.16	0.16

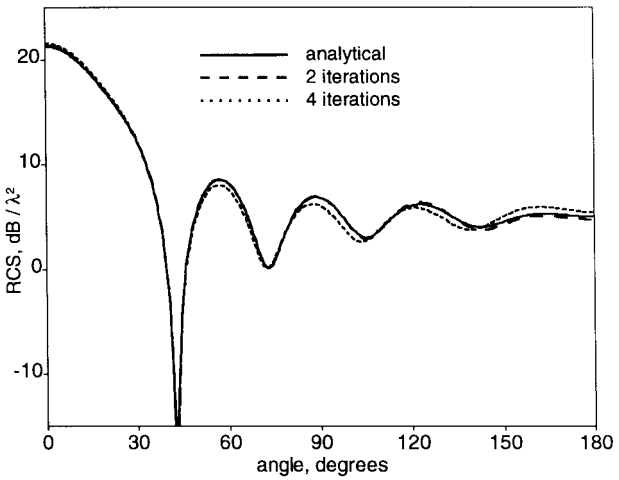

(a)

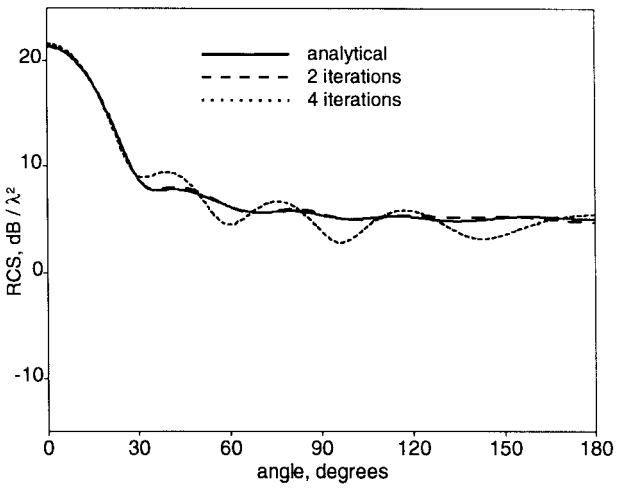

(b)

Fig. 4. Dual-surface CMT for sphere of radius λ, two and four one-way iterations. (a) Vertical plane pattern. (b) Horizontal plane pattern.

Table I shows the behavior of the solution when CMT is iterated, counting each one-way iteration (forward or backward) separately. The second column gives the maximum difference in the currents computed by successive iterations

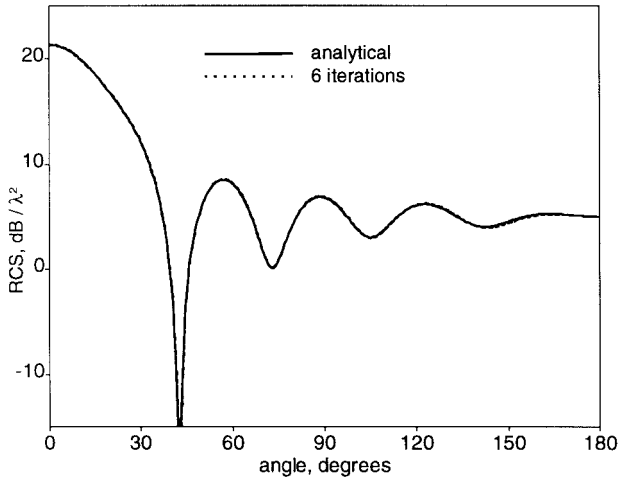

(a)

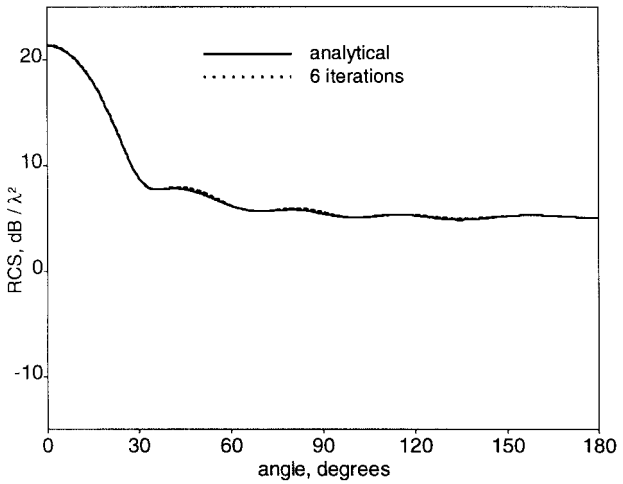

(b)

Fig. 5. Dual-surface CMT for sphere of radius λ, six one-way iterations. (a) Vertical plane pattern. (b) Horizontal plane pattern.

starting with zero current and using the 3-D Euclidean norm to measure magnitudes. Another useful quantity to look at is the maximum value of the magnetic field on the internal surface using the 3-D Euclidean norm again; this should tend to zero as the algorithm converges. Table I also gives the maximum deviation from the theoretical Mie solution in terms of far-field radiation pattern.

Table I shows that after the sixth iteration, the field inside the sphere no longer decreases significantly and the solution becomes stationary and the algorithm has essentially converged. The reason for a small error in results is discretization: we used the simplest pulse/delta functions approximation. Good agreement with theoretical results is in fact obtained after six iterations with a maximum error of less than 0.2 dB in both polarization plane patterns. These results are illustrated in Figs. 4 and 5, which show the dual-surface CMT results, respectively, for two and four one-way iterations and for six iterations. Execution time on a 200 MHz Pentium machine was less than 30 s for each iteration.

We now consider a metallic sphere of radius 5λ. Table II gives information on the convergence of the solution. Again

TABLE II
BEHAVIOR OF CMT SOLUTION FOR SPHERE OF RADIUS 5λ

Iter	Max current difference	Max internal magnetic field	Max error in radiation pattern for vertical plane (dB)	Max error in radiation pattern for horizontal plane (dB)
1	3.000	3.06	3.06	3.63
2	2.797	2.17	2.17	4.71
3	0.362	2.86	2.86	3.49
4	0.088	0.32	0.32	0.79
5	0.060	0.41	0.41	0.56
6	0.038	0.30	0.30	0.39

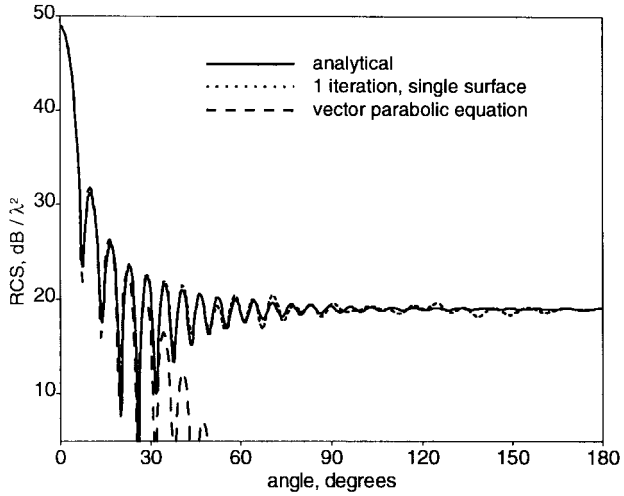

(a)

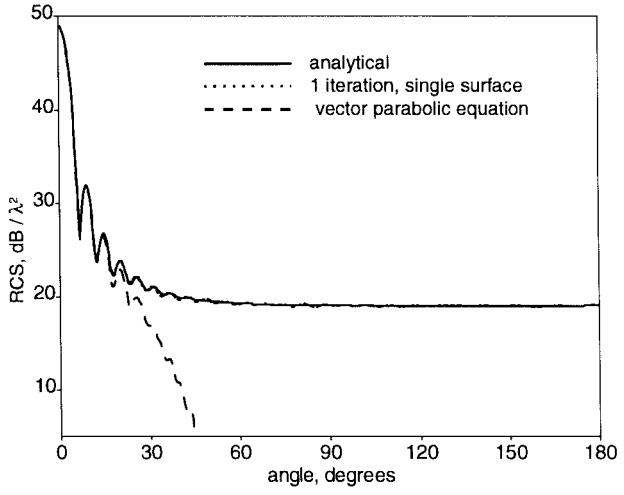

(b)

Fig. 6. Single iteration of CMT for sphere of radius 5λ. (a) Vertical plane pattern. (b) Horizontal plane pattern.

convergence is very fast; the accuracy limit is reached after six iterations as for the sphere or radius λ and the results compare very well to theory.

Fig. 6 shows SCMT results together with forward vector parabolic equation results and theoretical values. A single forward run of the vector parabolic equation algorithm [7]

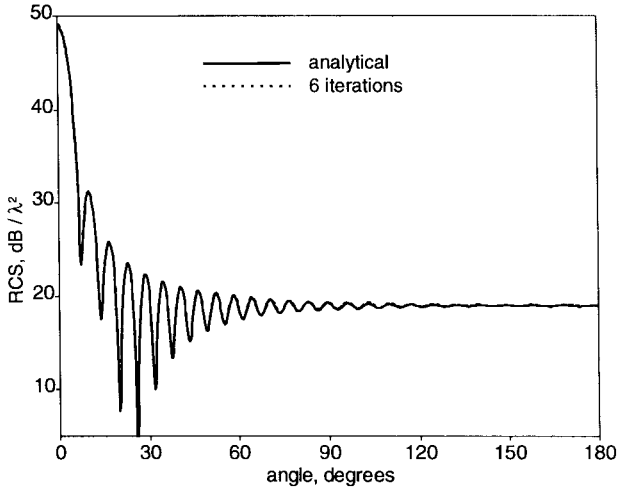

(a)

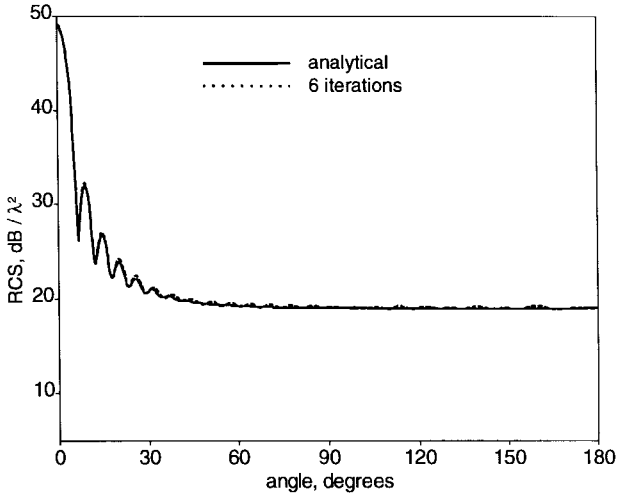

(b)

Fig. 7. Dual-surface CMT results for sphere of radius 5λ, six one-way iterations. (a) Vertical plane pattern. (b) Horizontal plane pattern.

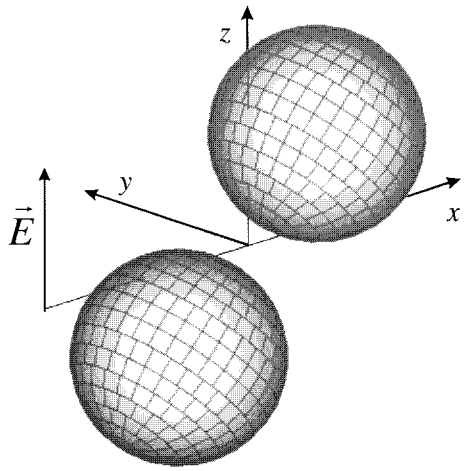

Fig. 8. Double sphere geometry.

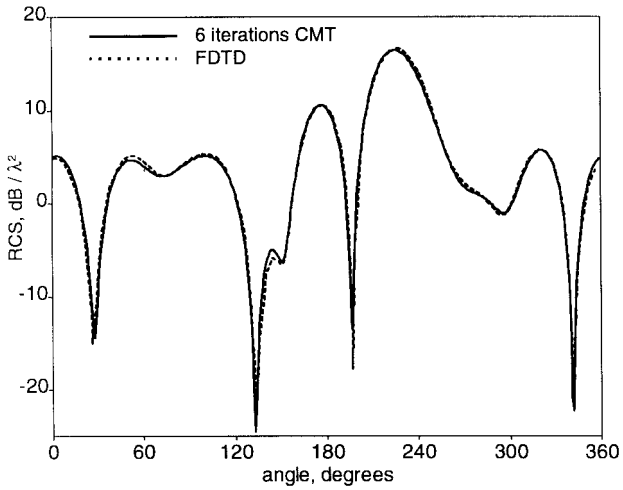

Fig. 9. CMT results for two spheres of radius $\lambda/2$ with centers separated by 1.25λ, six one-way iterations.

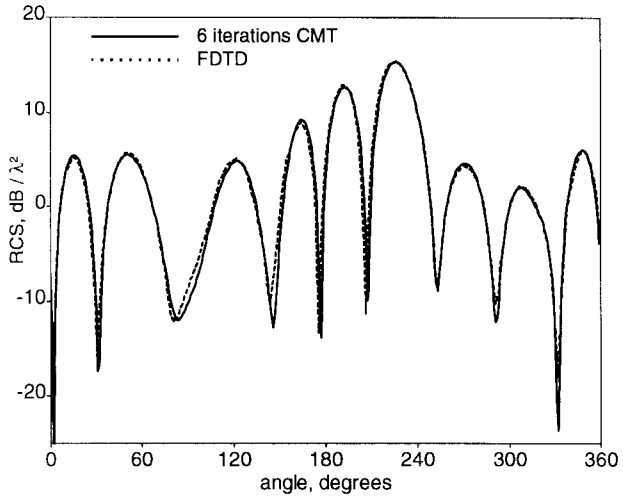

Fig. 10. CMT results for two spheres of radius $\lambda/2$ with centers separated 2λ, six one-way iterations.

produces accurate results in an angular cone of directions within 20° or so of the paraxial direction, because the method uses a narrow-angle approximation of the forward propagation operator. By contrast, very acceptable SCMT results are obtained at all scattering angles, which shows that SCMT provides an excellent high-frequency approximation.

Fig. 7 shows dual-surface CMT results for six iterations together with the theoretical results. Execution time on a 200 MHz Pentium machine was 4 h for each iteration. The results for 1λ and 5λ radius spheres give some indications that CMT convergence might not depend on object size.

The CMT works well with more complicated situations: we look at the case of two metallic spheres as shown in Fig. 8. Figs. 9 and 10 show RCS results obtained with five CMT iterations and with FDTD techniques [15] for two spheres of radius $\lambda/2$, with centers separated, respectively, by 1.25λ and 2λ. In these figures, the vertical plane pattern is plotted taking as the zero reference the forward direction joining the centers of the spheres, as in [15]. Agreement is excellent. In both cases, the small differences between the two methods could be due to the graphical extraction of FDTD results from [15]. For these examples, execution time for each iteration was less than

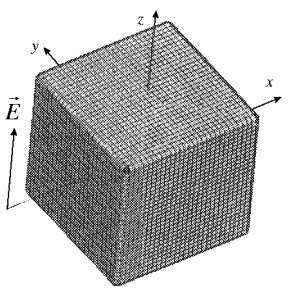

Fig. 11. Rounded cube.

TABLE III
BEHAVIOR OF CMT SOLUTION FOR SHARP-EDGED CUBE OF SIDE 3λ

Iter	Max current difference	Max internal magnetic field	Max difference with 10^{th} iteration radiation pattern for vertical plane (dB)	Max difference with 10^{th} iteration radiation pattern for horizontal plane (dB)
1	3.000	1.001	9.54	3.49
2	2.488	0.651	7.45	2.83
3	0.646	0.310	5.61	1.77
4	0.440	0.333	2.24	0.63
5	0.237	0.295	1.96	0.29
6	0.159	0.289	0.75	0.13
7	0.087	0.298	0.65	0.10
8	0.057	0.295	0.22	0.04
9	0.032	0.302	0.19	0.03
10	0.023	0.301	0.00	0.00

10 s. The accuracy limit was reached after the tenth iteration for both cases. Even though the object now has two convex components, the standard CMT still works, probably because no standing waves are generated between the two spheres.

Perfectly conducting cubes provide a challenging test, as they do not have symmetry of revolution and generate edge and corner diffraction. The fact that the surface is not smooth produces errors in the CMT solution, because of singular edge currents. We consider a cube of side 3λ under broadside plane wave incidence. To avoid numerical difficulties we tried replacing the sharp edges with rounded edges, using a radius of $\lambda/10$ for the edge cylinders and corner spherical caps, as shown in Fig. 11. Tables III and IV give the behavior of the solution for the sharp and rounded cubes, respectively, this time using the tenth iteration solution as a reference. The accuracy limit is reached after seven iterations for the rounded cube and the tenth iteration for the sharp-edged cube. It is interesting to note that convergence is faster for the rounded cube and also that the internal field decreases to much smaller values. For the sharp-edged cube, the edge singularities clearly affect the internal field, which remains substantial even after ten iterations. Fig. 12(a) and (b) shows bistatic RCS results in the horizontal and vertical planes, respectively. Results after six CMT iterations are shown for both the sharp and rounded cubes and DMFIE results graphically extracted from [9] are also shown for comparison. The sharp and rounded

TABLE IV
BEHAVIOR OF CMT SOLUTION FOR ROUNDED CUBE OF SIDE 3λ

Iter	Max current difference	Max internal magnetic field	Max difference with 10^{th} iteration radiation pattern for vertical plane (dB)	Max difference with 10^{th} iteration radiation pattern for horizontal plane (dB)
1	3.000	1.001	6.44	4.53
2	2.715	0.383	0.63	2.23
3	0.536	0.141	2.65	0.98
4	0.220	0.079	1.90	0.45
5	0.086	0.058	0.52	0.15
6	0.049	0.051	0.40	0.07
7	0.019	0.050	0.18	0.03
8	0.009	0.050	0.05	0.01
9	0.004	0.050	0.04	0.01
10	0.002	0.050	0.00	0.00

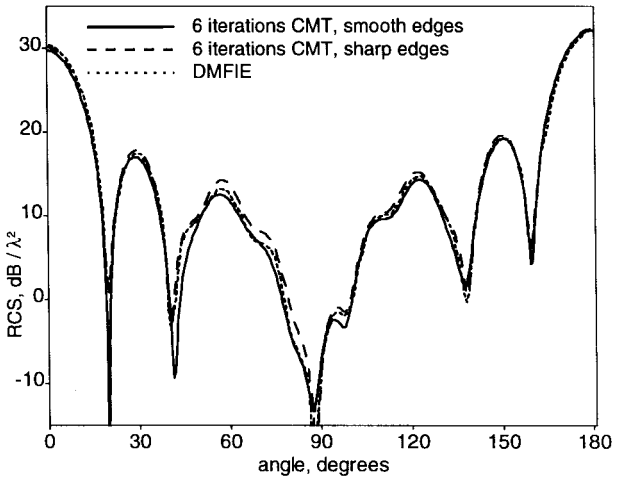

(a)

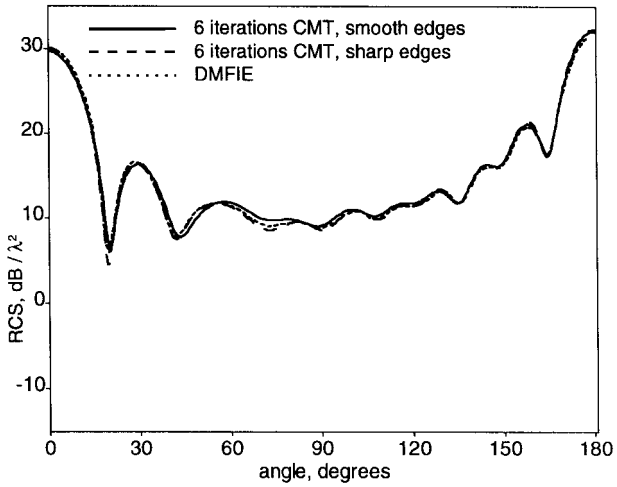

(b)

Fig. 12. CMT results for perfectly conducting cube of side 3λ, six one-way iterations. (a) Vertical plane pattern. (b) Horizontal plane pattern.

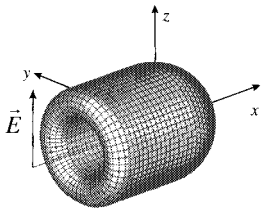

Fig. 13. Semi-open cavity. The inner and outer cylinder radii are 0.48λ and 0.96λ, cavity length 2.64λ.

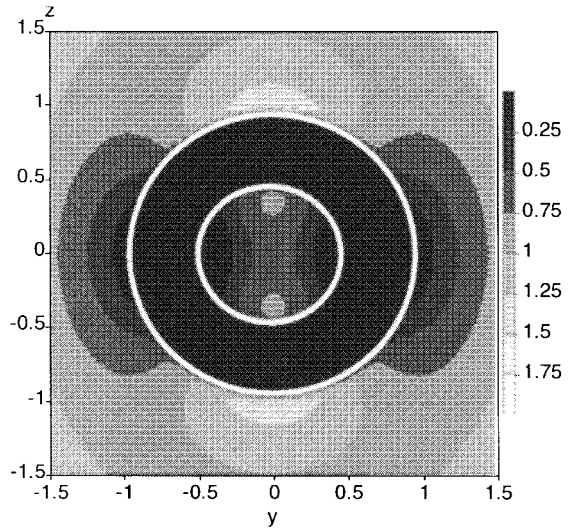

(a)

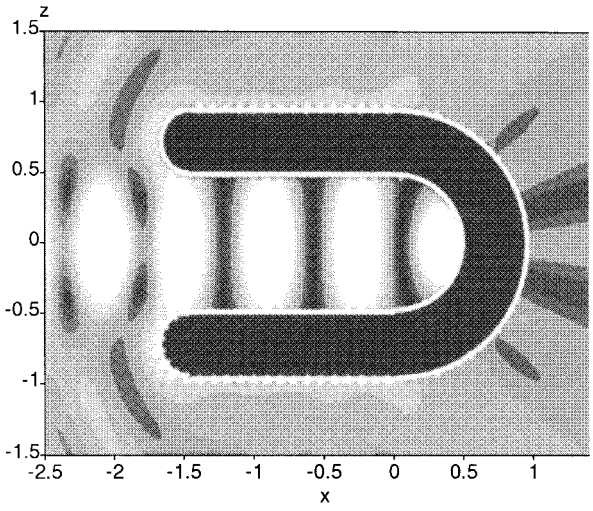

(b)

Fig. 14. Amplitude of the y component of magnetic field around the cavity after 20 one-way iterations. (a) $x = 0$ plane view. (b) $y = 0$ plane view.

cube solutions are noticeably different, showing the effect of the edges. The sharp cube CMT results are in better agreement with DMFIE results in the nulls, but the smooth cube results seem more accurate for facet scattering. For this case, each iteration took 7 min.

Finally, we treat the case of the cylindrical semi-open cavity shown in Fig. 13, closed by half-spheres and torus-shaped elements. For this nonconvex object, standing waves are formed inside the cavity. The standard CMT algorithm does not converge for this case and we used the modified CMT with a coefficient $t = 1/3$. This produced very satisfactory results (shown in Fig. 14), which give transverse and longitudinal views of the magnetic field inside the cavity. Table V shows the behavior of the algorithm; convergence is now slower and it takes about 20 iterations to reduce the far-field pattern differences to less than 0.1 dB. Of course, further work is required to test CMT on more general cavities, particularly on larger cavities supporting many modes.

An obvious question is whether one should use the modified CMT for all cases, since it seems that it always converges. The answer to this is that convergence is slightly slower for convex objects. In Tables VI and VII, we give the convergence properties of the CMT algorithm for a sphere of radius λ for values $1/2$ and $1/3$ of the conditioning parameter t, to conclude that the performance of the algorithm is very

TABLE V
BEHAVIOR OF CMT SOLUTION FOR SEMI-OPEN CAVITY

Iter	Max current difference	Max internal magnetic field	Max difference with 30th iteration radiation pattern for vertical plane (dB)	Max difference with 30th iteration radiation pattern for horizontal plane (dB)
1	2.000	0.981	11.17	18.18
2	2.804	0.479	14.06	11.38
3	0.996	0.387	11.75	14.40
4	0.663	0.223	7.53	5.05
5	0.335	0.193	4.72	2.30
6	0.226	0.167	3.10	1.44
7	0.175	0.114	1.32	1.52
8	0.110	0.091	1.27	0.81
9	0.121	0.074	0.82	0.93
10	0.068	0.071	0.91	0.54
15	0.017	0.075	0.18	0.15
20	0.005	0.080	0.06	0.04
25	0.002	0.080	0.03	0.01
30	0.001	0.079	0.00	0.00

TABLE VI
BEHAVIOR OF MODIFIED CMT ALGORITHM WITH $t = 1/2$ FOR SPHERE OF RADIUS λ

Iter	Max current difference	Max internal magnetic field	Max error in radiation pattern for vertical plane (dB)	Max error in radiation pattern for horizontal plane (dB)
1	2.000	0.999	5.87	9.03
2	2.905	0.467	3.12	6.25
3	0.694	0.227	1.90	2.62
4	0.212	0.187	1.24	1.54
5	0.318	0.107	1.21	0.73
6	0.103	0.087	0.85	0.43
7	0.103	0.049	0.70	0.25
8	0.042	0.043	0.41	0.21
9	0.033	0.036	0.29	0.19
10	0.015	0.033	0.18	0.18

TABLE VII
BEHAVIOR OF MODIFIED CMT ALGORITHM WITH $t = 1/3$ FOR SPHERE OF RADIUS λ

Iter	Max current difference	Max internal magnetic field	Max error in radiation pattern for vertical plane (dB)	Max error in radiation pattern for horizontal plane (dB)
1	2.000	0.999	3.27	4.10
2	2.844	0.259	1.36	2.53
3	0.402	0.105	0.90	0.61
4	0.128	0.065	0.50	0.29
5	0.106	0.039	0.47	0.18
6	0.035	0.035	0.22	0.16
7	0.020	0.034	0.17	0.16
8	0.007	0.033	0.15	0.16
9	0.003	0.033	0.16	0.16
10	0.002	0.033	0.16	0.16

slightly superior for $t = 0$. We suspect that this behavior could be explained in terms of potential theory: for example it is shown in [16] that the forward/backward double-layer potential operator is well behaved for convex objects, but not for nonconvex shapes. Performance is very good for $t = 1/3$, indicating that perhaps this value should be used whatever the shape of the object.

V. CONCLUSION

The current marching technique provides a solution to electromagnetic scattering problems for 3-D perfectly conducting objects. This is an iterative forward/backward marching method that converges in a small number of iterations. The dual-surface formulation avoids difficulties due to internal resonances and appropriate conditioning of the marching operator gives convergence for both convex and nonconvex objects. The initial results compare well with theory and other models for convex objects and first tests on cavities are encouraging. Due to the small number of iterations needed, it is possible to tradeoff between time and memory requirements and to treat large objects on personal computers.

At this point, we have not tried to optimize the speed of the CMT algorithm. It is likely that $N \log N$ CPU times per iteration are achievable with techniques similar to [1]. Current research is also focusing on speeding up the method using hybrid (combined with parabolic equation) techniques and extension of CMT to antenna modeling.

ACKNOWLEDGMENT

The authors would like to thank Dr. A. G. Voronovich for his contribution to the early stages of this work and many useful discussions.

REFERENCES

[1] W. C. Chew, J.-M. Jin, C.-C. Lu, E. Michielssen, and J. M. Song, "Fast solution methods in electromagnetics," *IEEE Trans. Antennas Propagat.*, vol. 45, pp. 533–543, Mar. 1997.

[2] D. A. Kapp and G. S. Brown, "A new numerical method for rough-surface scattering calculations," *IEEE Trans. Antennas Propagat.*, vol. 44, pp. 711–721, May 1996.

[3] D. Holliday, L. L. DeRaad Jr., and G. J. St-Cyr, "Forward-backward: A new method for computing low-grazing angle scattering," *IEEE Trans. Antennas Propagat.*, vol. 44, pp. 722–729, May 1996.

[4] P. Tran, "Calculation of the scattering of electromagnetic waves from a two-dimensional perfectly conducting surface using the method of ordered multiple interaction," *Waves Random Media*, vol. 7, no. 3, pp. 295–302, 1997.

[5] S. N. Makarov and M. Ochmann, "An iterative solver of the Helmholtz integral equation for high-frequency acoustic scattering," *J. Acoust. Soc. Amer.*, vol. 103, pp. 742–750, Feb. 1998.

[6] M. F. Levy and A. A. Zaporozhets, "Target scattering calculations with the parabolic equation method," *J. Acoust. Soc. Amer.*, vol. 103, pp. 735–741, Feb. 1998.

[7] A. A. Zaporozhets and M. F. Levy, "Bistatic RCS calculations with the vector parabolic equation method," *IEEE Trans. Antennas Propagat*, to be published.

[8] M. B. Woodworth and A. D. Yaghjian, "Derivation, application and conjugate gradient solutions of dual-surface integral equations for three-dimensional, mutli-wavelength perfect conductors," in *PIER 5*, J. A. Kong and T. K. Sarkar, Eds. New York: Elsevier, 1994, ch. 4.

[9] M. B. Woodworth and A. D. Yaghjian, "Multiwavelength three-dimensional scattering with dual-surface integral equations," *J. Opt. Soc. Amer.*, vol. 11, pp. 1399–1413, Apr. 1994.

[10] A. F. Peterson, "The "interior resonance" problem associated with surface integral equations of electromagnetics: Numerical consequences and a survey of remedies," *Electromagn.*, vol. 10, pp. 293–312, 1990.

[11] R. Barrett, M. Berry, T. F. Chan, J. Demmel, J. M. Donato, J. Dongarra, V. Eijkhout, R. Pozo, C. Romine, and H. Van der Vorst, *Templates for the Solution of Linear Systems: Building Blocks for Iterative Methods*. Philadelphia, PA: SIAM, 1994.

[12] D. Colton and R. Kress, *Integral Equation Methods in Scattering Theory*. Malabar, FL: Krieger, 1992.

[13] J.-P. Bérenger, "A perfectly matched layer for the absorption of electromagnetic waves," *J. Comp. Phys.*, vol. 114, pp. 185–200, Oct. 1994.

[14] J. J. Bowman, T. B. A. Senior, and P. L. E. Uslenghi, *Electromagnetic Scattering by Simple Shapes*, revised ed. New York: Hemisphere, 1987.

[15] T. G. Jurgens and A. Taflove, "Three-dimensional contour FDTD modeling of scattering from single and multiple bodies," *IEEE Trans. Antennas. Propagat.*, vol. 41, pp. 1703–1708, Dec. 1993.

[16] J. Král, *Integral Operators in Potential Theory*. New York: Springer-Verlag, 1980.

Andrew A. Zaporozhets was born in Moscow, Russia, in 1965. He received the Ph.D. degree in physics and mathematics from Moscow University, Russia, in 1991.

From 1992 to 1995, he was Visiting Research Fellow at the University of Southampton, U.K., where he worked on fast synthesis techniques for shaped reflector antennas. Since 1996 he has been with the Rutherford Appleton Laboratory, U.K. His main area of research work was antennas for microwave power transmission. He is currently working on marching techniques for the modeling of antennas, acoustical and radiowave propagation, and scattering.

Mireille F. Levy (M'96) received the M.Sc. degree in mathematics from the University Paris 7, France, in 1976, and the Ph.D. degree in mathematics from the University Paris 6, France, in 1980.

Her initial career was as a mathematician at the University Paris 6. In 1985 she joined the Radio Communications Research Unit, Rutherford Appleton Laboratory, Chilton, Didcot, U.K., where she is now in charge of the modeling group. She is also Head of the Ionospheric Group. She has worked on hybrid parabolic equation techniques for long-range radiowave applications, implementing models suitable for very large propagation domains. Her interests include short-term ionospheric forecasting and the development of marching methods for acoustic and electromagnetic scattering.

Dr. Levy is a member of the Institute of Electrical Engineers.